Finite element evaluation of diffusion and dispersion tensors in periodic porous media with advection

P. Tardif d'Hamonville[1], A. Ern[1] & L. Dormieux[2]

[1] *CERMICS, Ecole nationale des ponts et chaussées, 6-8 avenue Blaise Pascal, Champs sur Marne, 77455 Marne la Vallée Cedex 2, France*

[2] *LMSGC, Ecole nationale des ponts et chaussées, 6-8 avenue Blaise Pascal, Champs sur Marne, 77455 Marne la Vallée Cedex 2, France*

CERMICS — ENPC
6 et 8 avenue Blaise Pascal
Cité Descartes - Champs sur Marne
77455 Marne la Vallée Cedex 2

http://cermics.enpc.fr

FINITE ELEMENT EVALUATION OF DIFFUSION AND DISPERSION TENSORS IN PERIODIC POROUS MEDIA WITH ADVECTION

P. TARDIF D'HAMONVILLE[1], A. ERN[1], AND L. DORMIEUX[2]

Abstract. This paper presents three-dimensional finite element simulations to evaluate diffusion and dispersion tensors in periodic porous media in the presence of an advection velocity field. These tensors are evaluated in the framework of the double-scale expansion technique. Two problems, a Newtonian flow and a vector-valued advection–diffusion equation, have to be sequentially solved at the pore scale. Finite element techniques to approximate these problems are proposed and analyzed. Numerical results in three-dimensional networks of spheres are presented to quantitatively assess the impact of the pore morphology and of the advection velocity on the diffusion and dispersion tensors.

1. Introduction

The modelling of transport phenomena in porous media has been considered for a long time and can be traced back to Darcy's pioneering work which identified the pressure gradient as the driving force of fluid flow. The result of Darcy's phenomenological approach was the well-known linear relationship between the filtration velocity and the pressure gradient which is classically referred to as Darcy's law and which introduces the concept of permeability tensor. More recently, this law was given a micromechanical interpretation in the framework of periodic homogenization [8]. Darcy's law in fact appears as the macroscopic counterpart of Stokes equations written at the microscopic scale, i.e., that of the pores, and is widely used for the modelling of advection.

When the pore fluid is a mixture comprising a solvent and a solute, a relative motion of the solute with respect to the solvent can be activated whenever the concentration of the solute in the mixture is not homogeneous. Its driving force at the microscopic scale is the solute concentration gradient and its modelling at this scale goes back to Fick's law. This second mode of mass transport is referred to as diffusion [1]. When diffusion is not coupled with advection, the corresponding macroscopic transport law takes the form of a linear relationship between the macroscopic diffusive flux and the macroscopic gradient of solute concentration. This relationship is formally identical to the microscopic Fick law, except for the fact that the (scalar) diffusion coefficient is replaced by the homogenized tensor of diffusion which takes into account the tortuosity of the pore space. Estimates of this tensor can be derived by standard techniques [7].

Date: Draft version: 4th January 2006.

Key words and phrases. Double-scale expansion – periodic porous media – diffusion – dispersion – discrete divergence-free velocity – finite elements.

The present paper is devoted to the situation where diffusion is coupled with advection. In this case, in addition to the advective and diffusive terms, the flux of the solute comprises a dispersive term [5]. The periodic homogenization technique based on double-scale expansions provides an appropriate theoretical framework to relate the diffusion and dispersion tensors to the morphology of the pore space and to assess the influence of advection on them [3].

This paper is organized as follows. Section 2 briefly restates the theoretical framework of the double-scale expansion technique to evaluate the diffusion and dispersion tensors in periodic porous media with advection [3]. These tensors are evaluated by taking mean-values at the pore scale of a vector-valued field that solves a vector-valued advection–diffusion equation involving a velocity field that, in turn, solves a Stokes problem at the pore scale. Section 3 describes and analyzes various finite element techniques that can be used to approximate the fluid flow and the vector-valued advection–diffusion equations at the pore scale. Section 4 contains the numerical results. First, test cases with analytical solutions are considered to validate the methodology. Then, three-dimensional networks of spheres are investigated to quantify the impact of the pore morphology and of the advection velocity on the diffusion and dispersion tensors. Finally, Section 5 draws some conclusions.

2. Theoretical background

This section briefly restates the theoretical background based on periodic homogenization by double-scale expansion techniques to formulate the diffusion and dispersion tensors from the solution of problems posed at the pore scale. In this section, primes indicate non-dimensional quantities. Furthermore, the summation convention for repeated indices is adopted throughout the paper.

2.1. Notational preliminaries.

Let $(\underline{e}_1, \ldots, \underline{e}_d)$ denote the canonical basis of $\mathbb{R}^d$. Let $\underline{y} = (y_1, \ldots, y_d)$ denote the spatial coordinates in this basis. Consider a periodic porous medium with elementary parallelepipedic cell $\Omega = \prod_{i=1}^{d}[0, a_i]$ in $\mathbb{R}^d$. All the edge lengths a_i are of the order of the length scale ℓ that is characteristic of the medium heterogeneities. The elementary cell is embedded into a macroscopic structure of characteristic size L. The scale separation condition $\delta = \frac{\ell}{L} \ll 1$ means that the macro-structure comprises a large number of elementary cells.

The theory of periodic homogenization based on the double-scale expansion technique (see, e.g., [2]) classically regards any physical quantity $\mathcal{A}$, which is originally a function of $\underline{y}$, as a function of two new spatial coordinates $\underline{Z}' := \frac{1}{L}\underline{y}$ and $\underline{z}' := \frac{1}{\ell}\underline{y}$, i.e., $\mathcal{A}(\underline{y}) := \mathcal{A}(\underline{Z}', \underline{z}')$, in such a way that this function is periodic with respect to $\underline{z}'$. Accordingly, the dependence of $\mathcal{A}$ with respect to $\underline{z}'$ is related to fluctuations at the microscopic scale, i.e., within the elementary cell. In contrast, the dependence with respect to $\underline{Z}'$ takes into account the variations of $\mathcal{A}$ at the scale of the macroscopic structure. In the sequel, $\underline{\nabla}_y$ refers to the gradient operator with respect to the original spatial coordinates. In turn, $\underline{\nabla}_{Z'}$ and $\underline{\nabla}_{z'}$ are respectively associated with variations at the macroscopic scale and local fluctuations. These differential operators are related by the so-called chain rule $\underline{\nabla}_y = \frac{1}{L}\underline{\nabla}_{Z'} + \frac{1}{\ell}\underline{\nabla}_{z'}$.

The elementary cell Ω is partitioned into $\Omega = \Omega_{\mathrm{f}} \cup \Omega_{\mathrm{s}}$ where Ω_{f} denotes the volume occupied by the fluid phase and Ω_{s} that occupied by the solid phase. It is assumed that the solid phase is not deformed by the fluid flow. Furthermore, $\partial\Omega_{\mathrm{fs}}$ denotes the fluid–solid interface, i.e., $\partial\Omega_{\mathrm{fs}} = \partial\Omega_{\mathrm{f}} \cap \partial\Omega_{\mathrm{s}}$, and $\partial\Omega_{\mathrm{ff}}$ denotes the

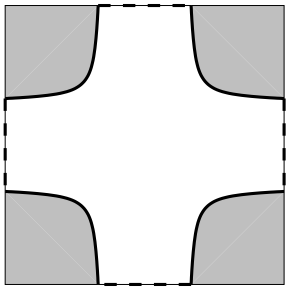

FIGURE 1. Elementary cell Ω in two dimensions; Ω_{s} is shaded in gray; $\partial\Omega_{\mathrm{fs}}$ consists of the four arcs drawn in bold; $\partial\Omega_{\mathrm{ff}}$ consists of the four segments indicated by a bold dashed line

fluid–fluid interface (that part of the fluid domain boundary where the fluid is in contact with the fluid in neighboring cells), i.e., $\partial\Omega_{\mathrm{ff}} = \partial\Omega_{\mathrm{f}} \setminus \partial\Omega_{\mathrm{fs}}$. The notation is illustrated in Figure 1. Set $\Omega' = \prod_{i=1}^{d}[0, \frac{a_i}{\ell}]$ and define Ω'_{f}, $\partial\Omega'_{\mathrm{fs}}$, and $\partial\Omega'_{\mathrm{ff}}$ as above.

Let $|\Omega'|$ denote the d-dimensional measure of the elementary cell Ω' and $|\Omega'_{\mathrm{f}}|$ that of Ω'_{f}. The ratio $\varphi = \frac{|\Omega'_{\mathrm{f}}|}{|\Omega'|}$ is the porosity of the medium. For a quantity $\omega(\underline{Z}', \underline{z}')$ attached to the fluid and thus defined on Ω'_{f} only, $\langle\omega\rangle_{\mathrm{f}}(\underline{Z}') = \frac{1}{|\Omega'|}\int_{\Omega'_{\mathrm{f}}} \omega(\underline{Z}', \underline{z}')d\underline{z}'$ denotes the apparent mean of ω and $\overline{\omega}^{\mathrm{f}} = \varphi^{-1}\langle\omega\rangle_{\mathrm{f}}$ its intrinsic mean. The fluctuation of a physical quantity ω defined on the fluid domain with respect to its intrinsic mean is defined as $\tilde{\omega} = \omega - \overline{\omega}^{\mathrm{f}}$.

2.2. **The flow problem.** Consider a stationary flow of a Newtonian fluid through the porous medium. The flow is driven by a macroscopic pressure gradient $\underline{\alpha}(\underline{Z})$. Denoting by μ the viscosity of the fluid, the flow is governed by the Stokes equations in the form

$$-\underline{\nabla}_y p + \mu\Delta_y u_i \underline{e}_i = \underline{0}, \tag{1}$$

$$\underline{\nabla}_y \cdot \underline{u} = 0. \tag{2}$$

Here, $\underline{u}$ denotes the velocity field and p the pressure field. It can be shown [2] that an expansion of the pressure p up to first order in the scale separation parameter δ yields

$$p(\underline{Z}, \underline{z}) = p_0(\underline{Z}) + \phi(\underline{Z}, \underline{z})\delta \quad \text{with } \overline{\phi}^{\mathrm{f}}(\underline{Z}) = 0, \tag{3}$$

that is, the leading order $p_0(\underline{Z})$ does not depend on $\underline{z}$, i.e., does not vary at the scale of an elementary cell. Accordingly, $\underline{\nabla}_Z p_0$ can be interpreted as the macroscopic pressure gradient $\underline{\alpha}$. In contrast, ϕ represents the fluctuation of the pressure at the scale of the elementary cell.

Define the non-dimensional velocity $\underline{u}'$ and pressure fluctuation ϕ' at the pore scale as

$$\underline{u}' = \frac{\mu}{\ell^2\alpha}\underline{u} \qquad \text{and} \qquad \phi' = \frac{1}{\alpha L}\phi, \tag{4}$$

where $\underline{\alpha} = \alpha \underline{e}_\alpha$ and α denotes the Euclidean norm of $\underline{\alpha}$. Introduction of (3) into (1), together with (2), yield

$$-\underline{\nabla}_{z'}\phi' + \Delta_{z'} u_i' \underline{e}_i = \underline{e}_\alpha \quad \text{on } \Omega_{\mathrm{f}}', \tag{5}$$

$$\underline{\nabla}_{z'} \cdot \underline{u}' = 0 \quad \text{on } \Omega_{\mathrm{f}}'. \tag{6}$$

The boundary conditions are

$$\underline{u}' = \underline{0} \quad \text{on } \partial\Omega_{\mathrm{fs}}', \tag{7}$$

$$\underline{u}' \text{ and } \phi' \text{ are } \underline{z}'\text{-periodic} \quad \text{on } \partial\Omega_{\mathrm{ff}}'. \tag{8}$$

Note that owing to (3), ϕ' has zero-mean over Ω_{f}'. Furthermore, since the above problem is linear, there is $\underline{\underline{k}}(\underline{z}')$ such that $\underline{u}' = -\underline{\underline{k}}(\underline{z}')\underline{e}_\alpha$. Switching back to dimensional quantities yields Darcy's law in the form

$$\overline{\underline{u}}^{\mathrm{f}} = -\frac{\ell^2}{\mu} \overline{\underline{\underline{k}}}^{\mathrm{f}} \cdot \underline{\nabla}_Z p_0. \tag{9}$$

The maximum norm in Ω_{f}' of the non-dimensional velocity $\underline{u}'$ solving (5)–(8) is denoted by $\Upsilon_{\max}$; it is a non-dimensional parameter depending only on the shape of Ω_{f}'. Typical values are of the order of 10^{-2}–10^{-3} for the problems of interest here. Accordingly, the flow velocity scale within the pore, say V_{F}, is given by

$$V_{\mathrm{F}} = \Upsilon_{\max} \frac{\alpha \ell^2}{\mu}. \tag{10}$$

To assess the validity of the Stokes equations to describe the fluid flow, i.e., to assess whether inertial effects are negligible with respect to diffusive effects, one computes the so-called Reynolds number such that

$$Re = \frac{\rho V_{\mathrm{F}} \ell}{\mu} = \Upsilon_{\max} \frac{\rho \alpha \ell^3}{\mu^2}, \tag{11}$$

where ρ is the density of the fluid. The validity of the Stokes regime is granted provided $Re \leq 1$, yielding an upper bound for the macroscopic pressure gradient in terms of the fluid properties and of the morphology of the porous medium, namely

$$\alpha \leq \frac{\mu^2}{\Upsilon_{\max} \rho \ell^3}. \tag{12}$$

As a numerical example, assume that the fluid is water so that $\rho \sim 10^3$ kg·m^{-3} and $\mu \sim 10^{-3}$ kg·m^{-1}·s^{-1}. Therefore, considering a pore scale of $\ell = 10^{-3}$ m yields $\alpha \leq 1$ kg·m^{-2}·s^{-2} if $\Upsilon_{\max} = 1$ and $\alpha \leq 10^2$ kg·m^{-2}·s^{-2} if $\Upsilon_{\max} = 10^{-2}$.

2.3. **The vector-valued advection–diffusion problem.** We consider a single chemical species γ diluted in a solvent that circulates in the porous medium. The (dimensional) velocity fields of the solvent and that of the solute are respectively denoted by $\underline{u}$ and $\underline{u}^\gamma$. Let D^γ denote the diffusion coefficient of the solute in the solvent. This coefficient, which refers to the diffusion of the solute through the solvent in an infinite fluid domain, is independent of the morphology of the porous medium. Fick's law relates the relative motion of the solute with respect to the solvent to the gradient of solute mass density ρ^γ as follows:

$$\underline{j}^\gamma_{\mathrm{diff}} = -D^\gamma \underline{\nabla}_y \rho^\gamma \tag{13}$$

where $\underline{j}^\gamma_{\rm diff} = \rho^\gamma(\underline{u}^\gamma - \underline{u})$ is the microscopic diffusive flux. The mass balance equation for the solute then reads as follows:

$$\partial_t \rho^\gamma + \underline{\nabla}_y \cdot (\rho^\gamma \underline{u} - D^\gamma \underline{\nabla}_y \rho^\gamma) = 0. \tag{14}$$

In order to discuss the influence of advection on the mass balance of the solute at the macroscopic level, it is convenient to introduce the reference velocity $V_{\rm D} = \frac{D^\gamma}{L}$. Three regimes can be identified (see [3]).

- The moderate advection regime in which $V_{\rm F} \leq V_{\rm D}$; in this regime, advection has no effect on the macroscopic description of diffusion, that is, dispersive effects are negligible with respect to diffusive effects.
- The advection dominated regime in which $V_{\rm F} \leq V_{\rm D}\delta^{-1}$; this regime constitutes the scope of the present work and is further discussed below.
- The non-homogenizable regime in which $V_{\rm F} \gg V_{\rm D}\delta^{-1}$.

Using (10), the advection dominated regime is characterized by the upper bound

$$\frac{V_{\rm F}\delta}{V_{\rm D}} = \frac{\Upsilon_{\max}\alpha\ell^3}{\mu D^\gamma} = Re\frac{\mu}{\rho D^\gamma} \leq 1, \tag{15}$$

where the Reynolds number is defined in (11). Recall that the macroscopic gradient α is chosen such that $Re \leq 1$; hence, a sufficient condition for the advection dominated regime to hold is $\frac{\mu}{\rho D^\gamma} \leq 1$.

We now focus on the advection dominated regime and we assume that the time scale of advection is of the same order of magnitude as the time scale of concentration changes. Using the double-scale expansion technique, it can be shown [3] that at the macroscopic scale, the mass balance of the solute is expressed as follows:

$$\partial_t \rho_0^\gamma + \underline{\nabla}_Z \cdot (\varphi \rho_0^\gamma \overline{\underline{u}}^{\rm f} + \underline{J}^\gamma_{\rm diff} + \underline{J}^\gamma_{\rm disp}) = 0, \tag{16}$$

with macroscopic diffusive and dispersive fluxes $\underline{J}^\gamma_{\rm diff}$ and $\underline{J}^\gamma_{\rm disp}$ given by

$$\underline{J}^\gamma_{\rm diff} = \varphi \overline{\underline{j}^\gamma_{\rm diff}}^{\rm f} \qquad \text{and} \qquad \underline{J}^\gamma_{\rm disp} = \varphi \overline{\tilde{\rho}^\gamma \tilde{\underline{u}}}^{\rm f}. \tag{17}$$

The expansion of the solute mass density ρ^γ up to first order in the scale separation parameter δ yields

$$\rho^\gamma(\underline{Z}, \underline{z}) = \rho_0^\gamma(\underline{Z}) + \rho_1^\gamma(\underline{Z}, \underline{z})\delta \quad \text{with } \overline{\rho_1^\gamma}^{\rm f}(\underline{Z}) = 0. \tag{18}$$

In other words, the leading term ρ_0^γ does not depend on the variable $\underline{z}$, that is, does not fluctuate at the scale of a cell. It only varies at the scale of the macroscopic structure and, as such, can be interpreted as the solute mass density at the macroscopic scale. In turn, the quantity ρ_1^γ represents the fluctuation at the cell scale and can be shown to be proportional to the macroscopic gradient of solute concentration. In other words, the following holds:

$$\rho_1^\gamma(\underline{Z}, \underline{z}) = \underline{\chi}(\underline{Z}, \underline{z}) \cdot \underline{\nabla}_Z \rho_0^\gamma(\underline{Z}) \quad \text{with } \overline{\underline{\chi}}^{\rm f}(\underline{Z}) = 0. \tag{19}$$

The field $\underline{\chi}$ can be evaluated by solving a vector-valued advection–diffusion problem at the pore scale which is conveniently written in non-dimensional form. Set $\underline{\chi}' = \frac{1}{L}\underline{\chi}$ and introduce the non-dimensional velocity field

$$\underline{u}'_\lambda = \frac{\delta}{V_{\rm D}}\underline{u} = \lambda \underline{u}' \quad \text{with } \lambda = \frac{\alpha\ell^3}{\mu D^\gamma}. \tag{20}$$

Condition (15) can be reformulated as

$$\lambda \leq \frac{1}{\Upsilon_{\max}}, \tag{21}$$

meaning that the maximum norm of the normalized velocity $\underline{u}'_\lambda$ is of the order of 1. Moreover, $\underline{\chi}'$ solves

$$-\Delta_{z'}\chi'_i\underline{e}_i + \underline{\underline{\nabla}}_{z'}\chi'\cdot\underline{u}'_\lambda = \overline{\underline{u}'_\lambda}^{\mathrm{f}} - \underline{u}'_\lambda \quad \text{on } \Omega'_{\mathrm{f}}, \tag{22}$$

subjected to the boundary conditions

$$\underline{\underline{\nabla}}_{z'}\chi'\cdot\underline{n} = -\underline{n} \qquad \text{on } \partial\Omega'_{\mathrm{fs}}, \tag{23}$$

$$\underline{\chi}' \text{ is } \underline{z}'\text{-periodic} \quad \text{on } \partial\Omega'_{\mathrm{ff}}, \tag{24}$$

where $\underline{n}$ is the unit outward normal to Ω'_{f}. A field $\underline{\chi}'$ solving (22)-(23)-(24) is only determined up to an additive constant. This arbitrariness is removed using the condition $\overline{\underline{\chi}'}^{\mathrm{f}} = 0$ stated in (19).

Switching back to dimensional variables, it is now possible to derive expressions of the macroscopic diffusive and dispersive fluxes in the form

$$\underline{J}^\gamma_{\mathrm{diff}} = -D^\gamma\underline{\underline{D}}^{\mathrm{diff}}\underline{\nabla}_Z\rho_0^\gamma \qquad \text{and} \qquad \underline{J}^\gamma_{\mathrm{disp}} = -D^\gamma\underline{\underline{D}}^{\mathrm{disp}}\underline{\nabla}_Z\rho_0^\gamma, \tag{25}$$

where the (non-dimensional) diffusion and dispersion tensors $\underline{\underline{D}}^{\mathrm{diff}}$ and $\underline{\underline{D}}^{\mathrm{disp}}$ are given by

$$\underline{\underline{D}}^{\mathrm{diff}} = \varphi\underline{\underline{T}} \qquad \text{with} \qquad \underline{\underline{T}} = \underline{\underline{I}} + \overline{(\underline{\underline{\nabla}}_{z'}\chi')^t}^{\mathrm{f}}, \tag{26}$$

where $\underline{\underline{I}}$ is the identity tensor, and

$$\underline{\underline{D}}^{\mathrm{disp}} = -\varphi\overline{\underline{u}'_\lambda\otimes\underline{\chi}'}^{\mathrm{f}}. \tag{27}$$

In the limit of zero advection, the tensor $\underline{\underline{T}}$ can be interpreted as the so-called tortuosity tensor.

3. Numerical methods

The problems (5)–(8) and (22)–(24) are solved approximately using finite element techniques. In the sequel, only problems posed in non-dimensional form on Ω'_{f} are considered; hence, primes are systematically omitted and the index z' is dropped from differential operators. Moreover, for any subset R of Ω_{f}, $\|\cdot\|_{0,R}$ denotes the canonical norm in $L^2(R)$ and for an integer $k \geq 1$, $\|\cdot\|_{k,R}$ denotes the canonical norm in the Sobolev space $H^k(R)$ (for simplicity, the same notation is employed for vector-valued functions). Furthermore, d denotes the space dimension; generally, $d = 3$, but in some instances, the case $d = 2$ is considered.

3.1. **The discrete setting.** Let $\{\mathcal{T}_h\}_{h>0}$ be a family of meshes of the fluid domain Ω_{f} consisting of simplices (triangles if $d = 2$ and tetrahedra if $d = 3$). The parameter h refers to the maximum mesh-size. Henceforth, c denotes a generic constant independent of h and whose numerical value can change at each occurrence. Set $H^1(\mathcal{T}_h) = \{q \in L^2(\Omega_{\mathrm{f}});\ \forall\tau \in \mathcal{T}_h,\ q|_\tau \in H^1(\tau)\}$.

Let $\widehat{\tau}$ be the reference simplex and for any mesh element $\tau \in \mathcal{T}_h$, let T_τ be the mapping from $\widehat{\tau}$ into τ. We assume that the meshes are affine; since only first-order finite elements are employed hereafter, this poses no restriction on accuracy in domains with curved boundaries. Moreover, we assume that the meshes do not contain hanging nodes. To enforce periodic boundary conditions on $\partial\Omega_{\mathrm{ff}}$, the

meshes are constructed in such a way that for all $i \in \{1, \dots, d\}$, the trace of $\mathcal{T}_h$ on the hyperplane $\{z_i = \frac{a_i}{\ell}\}$ is the image of the trace of $\mathcal{T}_h$ on the hyperplane $\{z_i = 0\}$ by the uniform translation of vector $\frac{a_i}{\ell}\underline{e}_i$.

For $\tau \in \mathcal{T}_h$, $\mathcal{F}(\tau)$ denotes the set of faces of τ; all the mesh faces are collected in the set $\mathcal{F}_h^\sharp = \bigcup_{\tau\in\mathcal{T}_h} \mathcal{F}(\tau)$. Owing to the particular nature of the boundary conditions addressed here, it is useful to distinguish various subsets of $\mathcal{F}_h^\sharp$.

- $\mathcal{F}_h^{\rm i}$ denotes the set of mesh interfaces, i.e., $F \in \mathcal{F}_h^{\rm i}$ if there are $\tau_1(F)$ and $\tau_2(F)$ in $\mathcal{T}_h$ such that $F = \tau_1(F) \cap \tau_2(F)$. For $F \in \mathcal{F}_h^{\rm i}$, $\underline{n}_F$ denotes the unit normal vector to F pointing from $\tau_1(F)$ towards $\tau_2(F)$, and $\mathcal{T}(F) = \{\tau_1(F), \tau_2(F)\}$. For a function $v \in H^1(\mathcal{T}_h)$, we define its jump across F as $[\![v]\!]_F = v|_{\tau_2(F)} - v|_{\tau_1(F)}$. The jump operator is extended to vector-valued functions using the same notation.
- $\mathcal{F}_h^{\rm fs}$ denotes the set of mesh faces located on $\partial\Omega_{\rm fs}$. For $F \in \mathcal{F}_h^{\rm fs}$, $\underline{n}_F$ denotes the unit normal vector to F pointing towards the exterior of $\Omega_{\rm f}$, $\tau(F)$ the mesh element of which F is a face, $\mathcal{T}(F) = \{\tau(F)\}$, and for $v \in H^1(\mathcal{T}_h)$, $[\![v]\!]_F = v|_{\tau(F)}$.
- By periodicity, the set of faces located on $\partial\Omega_{\rm ff}$ is divided into the subsets $\mathcal{F}_h^{\rm ff}$ and $\mathcal{F}_h^{\rm ff'}$. For $F \in \mathcal{F}_h^{\rm ff}$, we denote by $\tau_1(F)$ and $\tau_2(F)$ the two mesh elements sharing F by periodicity in such a way that $F \subset \partial\tau_1(F)$. Then, $\underline{n}_F$, $\mathcal{T}(F)$, and $[\![v]\!]_F$ are defined as for $F \in \mathcal{F}_h^{\rm i}$. For $F \in \mathcal{F}_h^{\rm ff'}$, $\underline{n}_F$ and $[\![v]\!]_F$ take the opposite values to those of the corresponding face in $\mathcal{F}_h^{\rm ff}$.
- It is also convenient to introduce the set $\mathcal{F}_h = \mathcal{F}_h^{\rm i} \cup \mathcal{F}_h^{\rm fs} \cup \mathcal{F}_h^{\rm ff}$.

For a face $F \in \mathcal{F}_h^\sharp$, h_F denotes its diameter and $|F|$ its $(d-1)$-dimensional measure. Similarly, for a mesh element $\tau \in \mathcal{T}_h$, h_τ denotes its diameter and $|\tau|$ its d-dimensional measure. For the purpose of the present simulations, it is sufficient to work with quasi-uniform mesh families; this means that there is c such that for all $F \in \mathcal{F}_h^\sharp$, $h \le c h_F$.

For an integer $k \ge 0$, let $\mathbb{P}_k$ denote the vector space of polynomials of total degree less than or equal to k. In the sequel, we shall use the following finite element spaces:

$$P_h^1 = \{v_h \in L^2(\Omega_{\rm f});\ \forall \tau \in \mathcal{T}_h,\ v_h|_\tau \in \mathbb{P}_1\}, \tag{28}$$

$$P_h^0 = \{v_h \in L^2(\Omega_{\rm f});\ \forall \tau \in \mathcal{T}_h,\ v_h|_\tau \in \mathbb{P}_0\}, \tag{29}$$

$$P_{{\rm Lag},h}^1 = \{v_h \in P_h^1;\ \forall F \in \mathcal{F}_h^{\rm i},\ [\![v_h]\!]_F = 0\}, \tag{30}$$

$$P_{{\rm Lag},h,0}^1 = \{v_h \in P_{{\rm Lag},h}^1;\ \forall F \in \mathcal{F}_h^{\rm fs} \cup \mathcal{F}_h^{\rm ff},\ [\![v_h]\!]_F = 0\}, \tag{31}$$

$$P_{{\rm CR},h}^1 = \{v_h \in P_h^1;\ \forall F \in \mathcal{F}_h^{\rm i},\ \textstyle\int_F [\![v_h]\!]_F = 0\}, \tag{32}$$

$$P_{{\rm CR},h,0}^1 = \{v_h \in P_{{\rm CR},h}^1;\ \forall F \in \mathcal{F}_h^{\rm fs} \cup \mathcal{F}_h^{\rm ff},\ \textstyle\int_F [\![v_h]\!]_F = 0\}. \tag{33}$$

P_h^1 is the space of piecewise affine functions, P_h^0 that of piecewise constant functions, $P_{{\rm Lag},h}^1$ the Lagrange finite element space of degree one, and $P_{{\rm CR},h}^1$ the so-called Crouzeix–Raviart finite element space. Recall the following trace and inverse trace inequalities: there is c such that for all $\tau \in \mathcal{T}_h$ and for all $v_h \in P_h^1$,

$$\|v_h\|_{0,F} \le c h_F^{-\frac{1}{2}} \|v_h\|_{0,\tau}, \tag{34}$$

$$\|v_h\|_{L^\infty(F)} \le c h_F^{-\frac{d-1}{2}} \|v_h\|_{0,F}, \tag{35}$$

where F is an arbitrary face of τ.

We introduce a local gradient operator $\underline{\nabla}_h$ such that for a function $v \in H^1(\mathcal{T}_h)$, its local gradient is defined for all $\tau \in \mathcal{T}_h$ as $(\underline{\nabla}_h v)|_\tau = \underline{\nabla}(v|_\tau)$. Similarly, for a vector-valued function $\underline{v} \in [H^1(\mathcal{T}_h)]^d$, its local divergence is defined for all $\tau \in \mathcal{T}_h$ as $(\underline{\nabla}_h \cdot \underline{v})|_\tau = \underline{\nabla} \cdot (\underline{v}|_\tau)$. Recall that in the distributional sense over Ω_f, the following holds:

$$\underline{\nabla} \cdot \underline{v} = \underline{\nabla}_h \cdot \underline{v} + \sum_{F \in \mathcal{F}_h^\mathrm{i}} [\![\underline{v}]\!]_F \cdot \underline{n}_F \delta_F, \tag{36}$$

where the second term in the right-hand side is a combination of Dirac delta functions that are interpreted as $\langle [\![\underline{v}]\!]_F \cdot \underline{n}_F \delta_F, \psi \rangle = \int_F [\![\underline{v}]\!]_F \cdot \underline{n}_F \psi$ where ψ is an arbitrary smooth function compactly supported in Ω_f.

3.2. **Finite element approximation of the flow problem.** To set the problem (5)–(8) in weak form, we introduce the spaces

$$V = \{\underline{v} \in [H^1(\Omega_\mathrm{f})]^d;\ \underline{v} = \underline{0} \text{ on } \partial\Omega_\mathrm{fs};\ \underline{v} \text{ is periodic on } \partial\Omega_\mathrm{ff}\}, \tag{37}$$

$$M = \{q \in L^2(\Omega_\mathrm{f});\ \textstyle\int_{\Omega_\mathrm{f}} q = 0\}. \tag{38}$$

Then, the flow problem consists of seeking $(\underline{u}, \phi) \in V \times M$ such that

$$\begin{cases} \displaystyle\int_{\Omega_\mathrm{f}} \underline{\underline{\nabla}} u : \underline{\underline{\nabla}} v - \int_{\Omega_\mathrm{f}} \phi \underline{\nabla} \cdot \underline{v} + \int_{\Omega_\mathrm{f}} \underline{e}_\alpha \cdot \underline{v} = 0, & \forall \underline{v} \in V, \\ \displaystyle\int_{\Omega_\mathrm{f}} \psi \underline{\nabla} \cdot \underline{u} = 0, & \forall \psi \in M. \end{cases} \tag{39}$$

It is straightforward to verify that this problem is well–posed.

Two classes of finite element methods can be employed to approximate (39), namely mixed finite element methods in which the velocity and the pressure finite element spaces satisfy a discrete inf-sup condition and stabilized finite elements in which the discrete inf-sup condition does not hold and least-squares terms are added to the weak formulation to control the residual; see, e.g., [9, p. 183–208]. For the purpose of comparison, one method in each class is considered. Equation (36) is useful to discuss the various finite element approximations. When working with stabilized conforming (i.e., continuous) finite elements, the second term in the right-hand side of (36) vanishes, but not the first owing to the presence of the stabilization term. When working with the mixed Crouzeix–Raviart/$\mathbb{P}_0$ finite element, the first term vanishes but not the second owing to the nonconformity of the discrete velocity space. In this second case, it is possible to design an accurate postprocessing of the discrete velocity field yielding continuity of the normal component across interfaces while preserving the local divergence, thus leading to a divergence-free discrete velocity field. Finally, since first-order finite elements will be employed to approximate the advection–diffusion problem (see §3.3), there is no point in utilizing a finite element method with accuracy larger than one to approximate the velocity field.

3.2.1. *Stabilized finite elements.* The main advantage of stabilized finite elements is ease of implementation since equal-order polynomial interpolation can be considered for both the velocity and the pressure. The approximate problem consists of seeking

$(\underline{u}_h, \phi_h) \in [P^1_{\mathrm{Lag},h,0}]^d \times P^1_{\mathrm{Lag},h,*}$ such that

$$\left\{\begin{array}{ll} \displaystyle\int_{\Omega_\mathrm{f}} \underline{\underline{\nabla}} u_h : \underline{\underline{\nabla}} v_h - \int_{\Omega_\mathrm{f}} \phi_h \underline{\nabla}\cdot\underline{v}_h + \int_{\Omega_\mathrm{f}} \underline{e}_\alpha \cdot \underline{v}_h = 0, & \forall \underline{v}_h \in [P^1_{\mathrm{Lag},h,0}]^d, \\ \displaystyle\int_{\Omega_\mathrm{f}} \psi_h \underline{\nabla}\cdot\underline{u}_h + \int_{\Omega_\mathrm{f}} c_{\mathrm{stab}} h^2 (\underline{\nabla}\phi_h + \underline{e}_\alpha)\cdot\underline{\nabla}\psi_h = 0, & \forall \psi_h \in P^1_{\mathrm{Lag},h,*}, \end{array}\right. \tag{40}$$

where $P^1_{\mathrm{Lag},h,*} = P^1_{\mathrm{Lag},h} \cap M$ ensures that functions in $P^1_{\mathrm{Lag},h,*}$ have zero-mean over Ω_f and $c_{\mathrm{stab}} \sim 1$ is a user-dependent constant independent of h. The above problem is well–posed and assuming elliptic regularity (this is generally the case since Ω_f has only convex corners) yields the following error estimate:

$$\|\underline{u} - \underline{u}_h\|_{0,\Omega_\mathrm{f}} + h\|\underline{\underline{\nabla}} u - \underline{\underline{\nabla}} u_h\|_{0,\Omega_\mathrm{f}} + h\|\phi - \phi_h\|_{0,\Omega_\mathrm{f}} \le ch^2. \tag{41}$$

Since $\underline{u}_h$ is continuous across interfaces, $\underline{\nabla}_h\cdot\underline{u}_h = \underline{\nabla}\cdot\underline{u}_h$; however, owing to the second equation in (40), $\underline{\nabla}\cdot\underline{u}_h \neq 0$.

3.2.2. *Mixed finite element methods.* To approximate (39) in a mixed setting, we consider the mixed Crouzeix–Raviart/$\mathbb{P}_0$ finite element. Thus, we seek $(\underline{u}_h, \phi_h) \in [P^1_{\mathrm{CR},h,0}]^d \times P^0_{h,*}$ such that

$$\left\{\begin{array}{ll} \displaystyle\int_{\Omega_\mathrm{f}} \underline{\underline{\nabla}_h} u_h : \underline{\underline{\nabla}_h} v_h - \int_{\Omega_\mathrm{f}} \phi_h \underline{\nabla}_h\cdot\underline{v}_h + \int_{\Omega_\mathrm{f}} \underline{e}_\alpha\cdot\underline{v}_h = 0, & \forall \underline{v}_h \in [P^1_{\mathrm{CR},h,0}]^d, \\ \displaystyle\int_{\Omega_\mathrm{f}} \psi_h \underline{\nabla}_h\cdot\underline{u}_h = 0, & \forall \psi_h \in P^0_{h,*}, \end{array}\right. \tag{42}$$

where $P^0_{h,*} = P^0_h \cap M$. The above problem is well–posed and assuming elliptic regularity yields the following error estimate:

$$\|\underline{u} - \underline{u}_h\|_{0,\Omega_\mathrm{f}} + h\|\underline{\underline{\nabla}} u - \underline{\underline{\nabla}}_h u_h\|_{0,\Omega_\mathrm{f}} + h\|\phi - \phi_h\|_{0,\Omega_\mathrm{f}} \le ch^2. \tag{43}$$

Owing to the second equation in (42), $\underline{\nabla}_h\cdot\underline{u}_h = 0$. However, because $\underline{u}_h$ is discontinuous across interfaces, $\underline{\nabla}\cdot\underline{u}_h \neq 0$. In the sequel, the following result is needed.

Lemma 3.1. *There is c such that*

$$\left(\sum_{F\in\mathcal{F}_h} \|[\![\underline{u}_h]\!]_F\|^2_{0,F}\right)^{\frac12} \le ch^{\frac32}. \tag{44}$$

Proof. Let $i_h\underline{u}$ be the Lagrange interpolant of the exact solution $\underline{u}$ in $P^1_{\mathrm{Lag},h}$. Using (34) yields for all $F \in \mathcal{F}_h$,

$$\begin{aligned} \|[\![\underline{u}_h]\!]_F\|_{0,F} = \|[\![\underline{u}_h - i_h\underline{u}]\!]_F\|_{0,F} &\le ch_F^{-\frac12}\|\underline{u}_h - i_h\underline{u}\|_{0,\mathcal{T}(F)} \\ &\le ch_F^{-\frac12}(\|\underline{u}_h - \underline{u}\|_{0,\mathcal{T}(F)} + \|\underline{u} - i_h\underline{u}\|_{0,\mathcal{T}(F)}). \end{aligned}$$

The conclusion follows by summing over mesh elements and using (43) as well as the approximation properties of the interpolation operator i_h. □

3.2.3. *A divergence-free projection of the discrete velocity field.* When solving the advection–diffusion problem, it is interesting to use a discrete velocity field which is divergence-free; see §3.3 for further discussion and §4.2 for numerical results. To this purpose, we design a projector from $[P^1_h]^d$ into $H(\mathrm{div};\Omega_\mathrm{f}) = \{\underline{v} \in [L^2(\Omega_\mathrm{f})]^d;\ \underline{\nabla}\cdot\underline{v} \in$

$L^2(\Omega_\mathrm{f})\}$ by using a technique closely inspired from [4]. Consider the so-called Brezzi–Douglas–Marini finite element space [6]

$$D_h = \{\underline{v}_h \in H(\mathrm{div};\Omega_\mathrm{f});\ \forall \tau \in \mathcal{T}_h,\ \underline{v}_h|_\tau \in [\mathbb{P}_1]^d\}. \tag{45}$$

For any face $\widehat{F}$ of the reference element $\widehat{\tau}$, let $(\widehat{p}_{\widehat{F},1},\dots,\widehat{p}_{\widehat{F},d})$ be a basis of $\mathbb{P}_1(\widehat{F})$. Then, for all $F \in \mathcal{F}_h^\sharp$, define $p_{F,i}(x) = \widehat{p}_{\widehat{F},i}(T_\tau^{-1}(x))$ for all $i \in \{1,\dots,d\}$ and $x \in F$, where τ is an element of which F is a face and $F = T_\tau(\widehat{F})$.

Let $F \in \mathcal{F}_h^\sharp$ and $i \in \{1,\dots,d\}$. For any function $\underline{v}_h$ that is single-valued on F, set

$$\sigma_{F,i}(\underline{v}_h) = \int_F (\underline{v}_h\cdot\underline{n}_F)p_{F,i}, \tag{46}$$

where $\underline{n}_F$ is already defined for $F \in \mathcal{F}_h$ and for $F \in \mathcal{F}_h^{\mathrm{ff}'}$, $\underline{n}_F$ is defined to be the unit normal vector pointing towards the exterior of Ω_f. In the sequel, we always choose $\widehat{p}_{\widehat{F},1} \equiv 1$ so that $\sigma_{F,1}(\underline{v}_h)$ is the mean-value of $(\underline{v}\cdot\underline{n}_F)$ over F.

Let $\tau \in \mathcal{T}_h$. There is a basis $(\underline{\theta}_{\tau,F,i})_{F\in\mathcal{F}(\tau),1\le i\le d}$ of $[\mathbb{P}_1(\tau)]^d$ such that for all $F,F' \in \mathcal{F}(\tau)$ and for all $i,i' \in \{1,\dots,d\}$, $\sigma_{F,i}(\underline{\theta}_{\tau,F',i'}) = \delta_{FF'}\delta_{ii'}$ where $\delta_{FF'}$ and $\delta_{ii'}$ are Kronecker symbols. For all $\underline{v}_h \in [P_h^1]^d$, observe that

$$\underline{v}_h = \sum_{\tau\in\mathcal{T}_h}\sum_{F\in\mathcal{F}(\tau)}\sum_{1\le i\le d}\sigma_{F,i}(\underline{v}_h|_\tau)\underline{\theta}_{\tau,F,i}. \tag{47}$$

Finally, define

$$\pi_h : [P_h^1]^d \ni \underline{v}_h \longmapsto \sum_{\tau\in\mathcal{T}_h}\sum_{F\in\mathcal{F}(\tau)}\sum_{1\le i\le d}\sigma_{F,i}(\{\underline{v}_h\}_F)\underline{\theta}_{\tau,F,i} \in D_h, \tag{48}$$

where $\{\underline{v}_h\}_F$ is the mean-value of $\underline{v}_h$ on F defined as $\{\underline{v}_h\}_F = \frac{1}{2}(\underline{v}_h|_{\tau_1(F)} + \underline{v}_h|_{\tau_2(F)})$ if $F \in \mathcal{F}_h^\sharp \setminus \mathcal{F}_h^{\mathrm{fs}}$, whereas $\{\underline{v}_h\}_F = 0$ if $F \in \mathcal{F}_h^{\mathrm{fs}}$.

Lemma 3.2. *Let $\underline{u}$ solve* (39) *and let $\underline{u}_h$ solve* (42)*. Then, the following holds:*

$$\underline{\nabla}\cdot(\pi_h\underline{u}_h) = 0, \tag{49}$$

$$\|\underline{u} - \pi_h\underline{u}_h\|_{0,\Omega_\mathrm{f}} \le ch^2. \tag{50}$$

Proof. (1) Let $\tau \in \mathcal{T}_h$. Since $\underline{u}_h \in [P^1_{\mathrm{CR},h}]^d$,

$$\begin{aligned}\int_\tau \underline{\nabla}\cdot(\pi_h\underline{u}_h) &= \sum_{F\in\mathcal{F}(\tau)}\int_F(\pi_h\underline{u}_h)\cdot\underline{n}_\tau = \sum_{F\in\mathcal{F}(\tau)}\int_F \epsilon_{\tau,F}\{\underline{u}_h\}_F\cdot\underline{n}_F\\ &= \sum_{F\in\mathcal{F}(\tau)}\int_F \underline{u}_h\cdot\underline{n}_\tau = \int_\tau \underline{\nabla}_h\cdot\underline{u}_h = 0,\end{aligned}$$

where $\epsilon_{\tau,F} = \underline{n}_\tau\cdot\underline{n}_F = \pm 1$, $\underline{n}_\tau$ being the outer normal to τ. Since $\underline{\nabla}\cdot(\pi_h\underline{u}_h)$ is constant on τ and $\pi_h\underline{u}_h \in H(\mathrm{div};\Omega_\mathrm{f})$, this proves (49).
(2) To prove (50), let $\tau \in \mathcal{T}_h$. For all $F \in \mathcal{F}(\tau)$ and for all $i \in \{1,\dots,d\}$, observe that $\|\underline{\theta}_{\tau,F,i}\|_{0,\tau} \le ch_\tau|\tau|^{-\frac{1}{2}}$. In addition, $\underline{u}_h|_\tau - \{\underline{u}_h\}_F = \epsilon_{\tau,F}\frac{1}{2}[\![\underline{u}_h]\!]_F$ if $F \in \mathcal{F}_h^\sharp\setminus\mathcal{F}_h^{\mathrm{fs}}$ and $\underline{u}_h|_\tau - \{\underline{u}_h\}_F = \underline{u}_h|_\tau$ if $F \in \mathcal{F}_h^{\mathrm{fs}}$. Hence, owing to (47) and (48),

$$\|\underline{u}_h - \pi_h\underline{u}_h\|_{0,\tau} \le c\sum_{F\in\mathcal{F}(\tau)}\sum_{1\le i\le d}\|[\![\underline{u}_h]\!]_F\|_{0,F}\|p_{F,i}\|_{0,F}h_\tau|\tau|^{-\frac{1}{2}}.$$

Using Lemma 3.1 and the fact that $\|p_{F,i}\|_{0,F} \le c|F|^{\frac{1}{2}}$ for all $F \in \mathcal{F}_h^\sharp$ yields $\|\underline{u}_h - \pi_h\underline{u}_h\|_{0,\Omega_\mathrm{f}} \le ch^2$, whence (50) follows using (43) and the triangle inequality. □

Remark 3.1. Using an inverse inequality, the triangle inequality, and estimate (41), it is readily inferred that $\|\underline{\underline{\nabla}}\underline{u} - \underline{\underline{\nabla}}_h(\pi_h\underline{u}_h)\|_{0,\Omega_\mathrm{f}} \le ch$. Also observe that the normal component of $\pi_h\underline{u}_h$ is exactly zero on $\partial\Omega_\mathrm{fs}$ and periodic over $\partial\Omega_\mathrm{ff}$. However, the tangential component of $\pi_h\underline{u}_h$ has no longer zero-mean on the faces of $\partial\Omega_\mathrm{fs}$. Using (34), it is inferred that $\|\underline{t}_F\cdot(\underline{u}_h - \pi_h\underline{u}_h)\|_{0,F} \le ch^{\frac{3}{2}}$ where $\underline{t}_F$ is a unit tangential vector to $F \in \mathcal{F}_h^\mathrm{fs}$, and hence $\frac{1}{|F|}|\int_F \underline{t}_F\cdot\pi_h\underline{u}_h| \le ch^{2-\frac{d}{2}} \le ch^{\frac{1}{2}}$ for $d \le 3$.

3.3. **Finite element approximation of the advection–diffusion problem.** To set the problem (22)–(24) in weak form, introduce the space

$$X = \{\underline{\chi} \in [H^1(\Omega_\mathrm{f})]^d;\ \underline{\chi} \text{ is periodic on } \partial\Omega_\mathrm{ff};\ \textstyle\int_{\Omega_\mathrm{f}} \underline{\chi} = \underline{0}\}, \tag{51}$$

as well as the forms

$$a(\underline{w};\underline{\chi},\underline{\psi}) = \int_{\Omega_\mathrm{f}} \underline{\underline{\nabla}}\underline{\chi}:\underline{\underline{\nabla}}\underline{\psi} + \int_{\Omega_\mathrm{f}} (\underline{\underline{\nabla}}\underline{\chi}\cdot\underline{w})\cdot\underline{\psi}, \tag{52}$$

$$b(\underline{w};\underline{\psi}) = \int_{\Omega_\mathrm{f}} (\overline{w}^\mathrm{f} - \underline{w})\cdot\underline{\psi} + \int_{\partial\Omega_\mathrm{fs}} \underline{\psi}\cdot\underline{n}, \tag{53}$$

where $\underline{w}$ is a given velocity field. In the sequel, we shall consider $\underline{w} = \underline{u}$ meaning that $\underline{w}$ solves the exact flow problem (39), $\underline{w} = \underline{u}_h^\mathrm{CR}$ meaning that $\underline{w} \in [P_{\mathrm{CR},h,0}]^d$ solves (42), $\underline{w} = \underline{u}_h^\mathrm{BDM}$ meaning that $\underline{w} \in D_h$ is the divergence-free projection of $\underline{u}_h^\mathrm{CR}$ constructed in §3.2.3, and $\underline{w} = \underline{u}_h^\mathrm{Lag}$ meaning that $\underline{w} \in [P^1_{\mathrm{Lag},h,0}]^d$ solves (40). Then, the advection–diffusion problem consists of seeking $\underline{\chi} \in X$ such that

$$a(\underline{w};\underline{\chi},\underline{\psi}) = b(\underline{w};\underline{\psi}), \qquad \forall\underline{\psi} \in X. \tag{54}$$

Before approximating (54), we address its well–posedness.

Lemma 3.3. *Problem* (54) *is well–posed if* $\underline{w} = \underline{u}$, *or if* $\underline{w} = \underline{u}_h^\mathrm{BDM}$, *or if* $\underline{w} = \underline{u}_h^\mathrm{CR}$ *and* h *is small enough, or if* $\underline{w} = \underline{u}_h^\mathrm{Lag}$, h *is small enough, and* $\|\underline{u}_h^\mathrm{Lag} - \underline{u}\|_{L^\infty(\Omega_\mathrm{f})} \le ch^{2-\frac{d}{2}}$.

Proof. The proof relies on the identity

$$a(\underline{w};\underline{\chi},\underline{\chi}) = \|\underline{\underline{\nabla}}\underline{\chi}\|_{0,\Omega_\mathrm{f}}^2 - \underbrace{\tfrac{1}{2}\int_{\Omega_\mathrm{f}} (\nabla_h\cdot\underline{w})\underline{\chi}^2}_{A} + \underbrace{\tfrac{1}{2}\sum_{F\in\mathcal{F}_h}\int_F (\llbracket\underline{w}\rrbracket_F\cdot\underline{n}_F)\underline{\chi}^2}_{B}, \tag{55}$$

and the Poincaré–Wirtinger inequality stating that $\|\underline{\underline{\nabla}}\underline{\chi}\|_{0,\Omega_\mathrm{f}} \ge c\|\underline{\chi}\|_{1,\Omega_\mathrm{f}}$ for all $\underline{\chi} \in X$. Recall also that owing to the standard trace inequality in $[H^1(\Omega_\mathrm{f})]^d$, for all $\tau \in \mathcal{T}_h$ and for all $F \in \mathcal{F}(\tau)$, $\|\underline{\chi}\|_{0,F} \le c\|\underline{\chi}\|_{1,\tau}$.
(1) If $\underline{w} = \underline{u}$ or if $\underline{w} = \underline{u}_h^\mathrm{BDM}$, then $A = B = 0$; hence, $a(\underline{w};\cdot,\cdot)$ is coercive on X and thus (54) is well–posed.
(2) If $\underline{w} = \underline{u}_h^\mathrm{CR}$, then $A = 0$. Moreover, using (35) and (44) yields

$$\begin{aligned}|B| &\le c\sum_{F\in\mathcal{F}_h} \|\llbracket\underline{w}\rrbracket_F\|_{L^\infty(F)}\|\underline{\chi}\|_{0,F}^2\\ &\le c\sum_{F\in\mathcal{F}_h} h_F^{-\frac{d-1}{2}}\|\llbracket\underline{w}\rrbracket_F\|_{0,F}\|\underline{\chi}\|_{1,\mathcal{T}(F)}^2 \le ch^{2-\frac{d}{2}}\|\underline{\underline{\nabla}}\underline{\chi}\|_{0,\Omega_\mathrm{f}}^2.\end{aligned}$$

Hence, $a(\underline{u}_h^{\mathrm{CR}};\underline{\chi},\underline{\chi}) \geq (1-ch^{2-\frac{d}{2}})\|\underline{\underline{\nabla}}\chi\|_{0,\Omega_\mathrm{f}}^2$.
(3) If $\underline{w} = \underline{v}_h^{\mathrm{Lag}}$, it is more convenient to work with (52). Observe that if $\underline{u}$ solves (39), then $\underline{u}$ is divergence-free and hence, $\int_{\Omega_\mathrm{f}}(\underline{\underline{\nabla}}\chi\cdot\underline{u})\cdot\underline{\chi} = 0$. This leads to

$$a(\underline{u}_h^{\mathrm{Lag}};\underline{\chi},\underline{\chi}) = \|\underline{\underline{\nabla}}\chi\|_{0,\Omega_\mathrm{f}}^2 + \int_{\Omega_\mathrm{f}}(\underline{\underline{\nabla}}\chi\cdot(\underline{u}_h^{\mathrm{Lag}}-\underline{u}))\cdot\underline{\chi}.$$

Since $\|\underline{u}_h^{\mathrm{Lag}}-\underline{u}\|_{L^\infty(\Omega_\mathrm{f})} \leq ch^{2-\frac{d}{2}}$, $a(\underline{u}_h^{\mathrm{Lag}};\underline{\chi},\underline{\chi}) \geq (1-ch^{2-\frac{d}{2}})\|\underline{\underline{\nabla}}\chi\|_{0,\Omega_\mathrm{f}}^2$. □

Remark 3.2. The hypothesis $\|\underline{u}_h^{\mathrm{Lag}}-\underline{u}\|_{L^\infty(\Omega_\mathrm{f})} \leq ch^{2-\frac{d}{2}}$ is very weak; in general, second-order convergence is observed in the $L^\infty(\Omega_\mathrm{f})$-norm.

We now turn to the finite element approximation of (54). We consider Lagrange finite elements of degree one. Owing to (21), the velocity norm is always less than one; hence, in the vocabulary of finite elements, (54) is in the so-called dominant diffusion regime, and no stabilization of advective derivatives is needed. Let

$$X_h = \{\underline{\chi}_h \in [P^1_{\mathrm{Lag},h}]^d;\ \forall F\in\mathcal{F}_h^{\mathrm{ff}},\ [\![\underline{\chi}_h]\!]_F = 0;\ \textstyle\int_{\Omega_\mathrm{f}}\underline{\chi}_h = \underline{0}\}. \tag{56}$$

Note that functions in X_h are periodic on $\partial\Omega_{\mathrm{ff}}$. Then, the discrete problem consists of seeking $\underline{\chi}_h \in X_h$ such that

$$a(\underline{w}_h;\underline{\chi}_h,\underline{\psi}_h) = b(\underline{w}_h;\underline{\psi}_h), \qquad \forall\underline{\psi}_h \in X_h. \tag{57}$$

Here, $\underline{w}_h$ is one of the three finite element approximations of the velocity field discussed above. Since $X_h \subset X$, (57) is well–posed under the assumptions of Lemma 3.3.

Theorem 3.1. *Let $\underline{\chi}$ solve (54) with $\underline{w} = \underline{u}$ and assume $\underline{\chi} \in [H^2(\Omega_\mathrm{f})]^d$. Let $\underline{\chi}_h$ solve (57) with $\underline{w}_h$ equal to $\underline{u}_h^{\mathrm{BDM}}$, $\underline{u}_h^{\mathrm{CR}}$, or $\underline{u}_h^{\mathrm{Lag}}$. Then, the following holds:*

$$\|\underline{\chi}-\underline{\chi}_h\|_{1,\Omega_\mathrm{f}} \leq ch. \tag{58}$$

Proof. Since $\underline{\chi} \in [H^2(\Omega_\mathrm{f})]^d$ and $d\leq 3$, $\underline{\chi}$ is continuous and bounded on Ω_f. Let $i_h\underline{\chi}$ denote the Lagrange interpolant of $\underline{\chi}$ in $[P^1_{\mathrm{Lag},h}]^d$. Let $\underline{w}_h$ be taken equal to $\underline{u}_h^{\mathrm{BDM}}$, $\underline{u}_h^{\mathrm{CR}}$, or $\underline{u}_h^{\mathrm{Lag}}$. The proof of (58) relies on the First Strang Lemma which yields the following estimate:

$$\begin{aligned} c\|\underline{\chi}-\underline{\chi}_h\|_{1,\Omega_\mathrm{f}} \leq \|\underline{\chi}-i_h\underline{\chi}\|_{1,\Omega_\mathrm{f}} &+ \sup_{\underline{\psi}_h\in X_h}\frac{a(\underline{u};i_h\underline{\chi},\underline{\psi}_h)-a(\underline{w}_h;i_h\underline{\chi},\underline{\psi}_h)}{\|\underline{\psi}_h\|_{1,\Omega_\mathrm{f}}} \\ &+ \sup_{\underline{\psi}_h\in X_h}\frac{b(\underline{u};\underline{\psi}_h)-b(\underline{w}_h;\underline{\psi}_h)}{\|\underline{\psi}_h\|_{1,\Omega_\mathrm{f}}} \equiv T_1+T_2+T_3. \end{aligned}$$

(1) Clearly, $|T_1| \leq ch$.
(2) To estimate the second term, observe that

$$\begin{aligned} &a(\underline{u};i_h\underline{\chi},\underline{\psi}_h)-a(\underline{w}_h;i_h\underline{\chi},\underline{\psi}_h) = \int_{\Omega_\mathrm{f}}(\underline{\underline{\nabla}}i_h\chi\cdot(\underline{u}-\underline{w}_h))\cdot\underline{\psi}_h \\ &= -\int_{\Omega_\mathrm{f}}(\underline{\underline{\nabla}}\psi_h\cdot(\underline{u}-\underline{w}_h))\cdot i_h\underline{\chi} - \int_{\Omega_\mathrm{f}}(\underline{\nabla}_h\cdot\underline{w}_h)(\underline{\psi}_h\cdot i_h\underline{\chi}) + \sum_{F\in\mathcal{F}_h}\int_F[\![\underline{w}_h]\!]_F\cdot\underline{n}_F(\underline{\psi}_h\cdot i_h\underline{\chi}) \\ &\equiv T_{2,1}+T_{2,2}+T_{2,3}. \end{aligned}$$

Clearly, $|T_{2,1}| \le c\|\underline{\underline{\nabla}}\psi_h\|_{0,\Omega_\mathrm{f}}\|\underline{u}-\underline{w}_h\|_{0,\Omega_\mathrm{f}}\|i_h\underline{\chi}\|_{[L^\infty(\Omega_\mathrm{f})]^d} \le ch^2\|\underline{\psi}_h\|_{1,\Omega_\mathrm{f}}$.
(2.a) If $\underline{w}_h = \underline{u}_h^{\mathrm{BDM}}$, then $T_{2,2} = T_{2,3} = 0$.
(2.b) If $\underline{w}_h = \underline{u}_h^{\mathrm{CR}}$, then $T_{2,2} = 0$ and owing to (34) and (44),

$$|T_{2,3}| \le c\sum_{F\in\mathcal{F}_h} \|[\![\underline{u}_h^{\mathrm{CR}}]\!]_F\|_{0,F}h_F^{-\frac{1}{2}}\|\underline{\psi}_h\|_{0,\mathcal{T}(F)}\|i_h\underline{\chi}\|_{[L^\infty(F)]^d} \le ch\|\underline{\psi}_h\|_{1,\Omega_\mathrm{f}}.$$

(2.c) If $\underline{w}_h = \underline{u}_h^{\mathrm{Lag}}$, then $T_{2,3} = 0$ and

$$|T_{2,2}| \le \|\underline{\nabla}_h\cdot\underline{u}_h^{\mathrm{Lag}}\|_{0,\Omega_\mathrm{f}}\|\underline{\psi}_h\|_{0,\Omega_\mathrm{f}}\|i_h\underline{\chi}\|_{[L^\infty(\Omega_\mathrm{f})]^d} \le ch\|\underline{\psi}_h\|_{1,\Omega_\mathrm{f}}.$$

(3) To estimate the third term, observe that

$$b(\underline{u};\underline{\psi}_h) - b(\underline{w}_h;\underline{\psi}_h) = \int_{\Omega_\mathrm{f}} (\overline{\underline{u}}^{\mathrm{f}} - \underline{u} - \overline{\underline{w}_h}^{\mathrm{f}} + \underline{w}_h)\cdot\underline{\psi}_h.$$

Since $\|\overline{\underline{u}}^{\mathrm{f}} - \overline{\underline{w}_h}^{\mathrm{f}}\|_{0,\Omega_\mathrm{f}} \le \|\underline{u}-\underline{w}_h\|_{0,\Omega_\mathrm{f}} \le ch^2$, it is clear that $|T_3| \le ch^2$. □

To complete the analysis, we derive an error estimate in the L^2-norm using the duality technique of the Aubin–Nitsche lemma. To this purpose, we consider the adjoint problem which consists of seeking $\underline{\Xi} \in X$ such that

$$a(\underline{u};\underline{\psi},\underline{\Xi}) = (\underline{\chi}-\underline{\chi}_h,\underline{\psi})_{\Omega_\mathrm{f}}, \qquad \forall\underline{\psi}\in X, \tag{59}$$

where $\underline{\chi}$ solves (54) with $\underline{w} = \underline{u}$ and $\underline{\chi}_h$ solves (57) with $\underline{w}_h$ equal to $\underline{u}_h^{\mathrm{BDM}}$, $\underline{u}_h^{\mathrm{CR}}$, or $\underline{u}_h^{\mathrm{Lag}}$. We assume that the above problem yields elliptic regularity, i.e., there is c such that

$$\|\underline{\Xi}\|_{2,\Omega_\mathrm{f}} \le c\|\underline{\chi}-\underline{\chi}_h\|_{0,\Omega_\mathrm{f}}. \tag{60}$$

Theorem 3.2. *In the above framework, the following holds:*

$$\|\underline{\chi}-\underline{\chi}_h\|_{0,\Omega_\mathrm{f}} \le c(h\|\underline{\chi}-\underline{\chi}_h\|_{1,\Omega_\mathrm{f}} + h^2). \tag{61}$$

Proof. Since $\underline{\Xi}$ solves (59), testing with $\underline{\psi} = \underline{\chi}-\underline{\chi}_h$ yields

$$\begin{aligned}
\|\underline{\chi}-\underline{\chi}_h\|_{\Omega_\mathrm{f}}^2 &= a(\underline{u};\underline{\chi}-\underline{\chi}_h,\underline{\Xi}) \\
&= a(\underline{u};\underline{\chi}-\underline{\chi}_h,\underline{\Xi}-\underline{\psi}_h) + a(\underline{u};\underline{\chi}-\underline{\chi}_h,\underline{\psi}_h) \\
&= a(\underline{u};\underline{\chi}-\underline{\chi}_h,\underline{\Xi}-\underline{\psi}_h) + [a(\underline{w}_h;\underline{\chi}_h,\underline{\psi}_h) - a(\underline{u};\underline{\chi}_h,\underline{\psi}_h)] \\
&\quad + [b(\underline{u};\underline{\psi}_h) - b(\underline{w}_h;\underline{\psi}_h)] \equiv T_1 + T_2 + T_3,
\end{aligned}$$

where $\underline{\psi}_h$ is arbitrary in X_h and where $\underline{w}_h$ is taken equal to $\underline{u}_h^{\mathrm{BDM}}$, $\underline{u}_h^{\mathrm{CR}}$, or $\underline{u}_h^{\mathrm{Lag}}$. Since $\underline{\Xi} \in [H^2(\Omega_\mathrm{f})]^d$ and $d \le 3$, $\underline{\Xi}$ is continuous and bounded on Ω_f. Take $\underline{\psi}_h = i_h\underline{\Xi}$, the Lagrange interpolant of $\underline{\Xi}$ in $[P^1_{\mathrm{Lag},h}]^d$.
(1) Owing to (60) and classical interpolation properties of i_h,

$$|T_1| \le c\|\underline{\chi}-\underline{\chi}_h\|_{1,\Omega_\mathrm{f}}h\|\underline{\Xi}\|_{2,\Omega_\mathrm{f}} \le ch\|\underline{\chi}-\underline{\chi}_h\|_{1,\Omega_\mathrm{f}}\|\underline{\chi}-\underline{\chi}_h\|_{0,\Omega_\mathrm{f}}.$$

(2) Since $\|\underline{\psi}_h\|_{[L^\infty(\Omega_\mathrm{f})]^d} \le c\|\underline{\Xi}\|_{2,\Omega_\mathrm{f}} \le c\|\underline{\chi}-\underline{\chi}_h\|_{0,\Omega_\mathrm{f}}$ and $\|\underline{\underline{\nabla}}\chi_h\|_{0,\Omega_\mathrm{f}} \le c$,

$$|T_2| \le \|\underline{\underline{\nabla}}\chi_h\|_{0,\Omega_\mathrm{f}}\|\underline{u}-\underline{w}_h\|_{0,\Omega_\mathrm{f}}\|\underline{\psi}_h\|_{[L^\infty(\Omega_\mathrm{f})]^d} \le ch^2\|\underline{\chi}-\underline{\chi}_h\|_{0,\Omega_\mathrm{f}}.$$

(3) Finally,

$$|T_3| \le ch^2\|\underline{\psi}_h\|_{0,\Omega_\mathrm{f}} \le ch^2\|\underline{\Xi}\|_{2,\Omega_\mathrm{f}} \le ch^2\|\underline{\chi}-\underline{\chi}_h\|_{0,\Omega_\mathrm{f}}.$$

The conclusion is straightforward. □

Combining the estimates of Theorems 3.1 and 3.2 with (26) and (27) shows that with the three finite element techniques for the velocity field, the approximation for the diffusion tensor converges to first-order in the mesh-size and the approximation for the dispersion tensor converges to second-order in the mesh-size.

3.4. **Implementation aspects.** This section briefly reviews some implementation aspects of the finite element approximations analyzed in the previous sections.

For the Stokes problem, it is convenient to discard the global constraint $\int_{\Omega_\mathrm{f}} \phi_h = 0$ to work with finite element spaces having localized basis functions. Hence, $P^0_{h,*}$ (resp., $P^1_{\mathrm{Lag},h,*}$) is replaced by P^0_h (resp., $P^1_{\mathrm{Lag},h}$) in (42) (resp., (40)). An approximate solution to the linear system is obtained using the Uzawa algorithm and the conjugate gradient method to solve the velocity subsystem (resp., the GMRes algorithm to solve the pressure–velocity system). Upon convergence, the discrete pressure field can be filtered to ensure the zero-mean constraint.

For the advection–diffusion problem, the same motivation pleads for using the finite element space

$$Y_h = \{\underline{\chi}_h \in [P^1_{\mathrm{Lag},h}]^d;\ \forall F \in \mathcal{F}_h^{\mathrm{ff}},\ [\![\underline{\chi}_h]\!]_F = 0\}, \tag{62}$$

instead of X_h in (57). When the discrete velocity field is divergence-free, i.e., for $\underline{w}_h = \underline{u}_h^{\mathrm{BDM}}$, this poses no problem since it is straightforward to verify the following

Lemma 3.4. *Let $\underline{w}_h$ be a divergence-free velocity field.*
(i) *If $\underline{\chi}_h$ solves* (57)*, then $\forall \underline{\kappa} \in \mathbb{R}^d$, $\underline{\chi}'_h = \underline{\chi}_h + \underline{\kappa}$ is in Y_h and such that*

$$a(\underline{w}_h; \underline{\chi}'_h, \underline{\psi}_h) = b(\underline{w}_h; \underline{\psi}_h), \qquad \forall \underline{\psi}_h \in Y_h. \tag{63}$$

(ii) *Conversely, if $\underline{\chi}'_h \in Y_h$ solves* (63)*, then $\underline{\chi}_h = \underline{\chi}'_h - \frac{1}{|\Omega_\mathrm{f}|}\int_{\Omega_\mathrm{f}} \underline{\chi}'_h \in X_h$ is the unique solution of* (57)*.*

When working with the linear system associated with (63), an approximate solution can be obtained using the GMRes algorithm and upon convergence, the zero-mean constraint on $\underline{\chi}_h$ is enforced by filtering. However, when the discrete velocity field is no longer divergence-free, i.e., for $\underline{w}_h = \underline{u}_h^{\mathrm{CR}}$ or for $\underline{w}_h = \underline{u}_h^{\mathrm{Lag}}$, the linear system associated with (63) does not admit any solution. This results from the fact that for any constant field $\underline{\kappa}$ in Ω_f,

$$b(\underline{w}_h; \underline{\kappa}) = 0 \qquad \text{and} \qquad a(\underline{w}_h; \underline{\chi}'_h, \underline{\kappa}) \neq 0, \tag{64}$$

in general (whereas $a(\underline{w}_h; \underline{\chi}'_h, \underline{\kappa}) = 0$ if $\underline{w}_h$ is divergence-free). In practice, it is still possible to employ the GMRes algorithm to find the discrete field $\underline{\chi}'_h$ that minimizes the Euclidean norm of the residual associated with the linear system, but this procedure can result in a loss of accuracy when evaluating the diffusion and dispersion tensors since it is not known a priori to which level the linear system residual can be minimized. A quantitative discussion is postponed to §4.

4. Results

This section presents numerical results, first on analytical test cases to validate the convergence analysis and then on three-dimensional sphere networks to assess quantitatively the impact of the pore morphology and of the advection velocity on macroscopic diffusive and dispersive transport. As in the previous section, only problems in non-dimensional form are considered and primes are omitted.

	Stokes			advection–diffusion	
i	$\|\underline{u}-\underline{u}_h\|_{0,\Omega_\mathrm{f}}$	$\|\underline{u}-\underline{u}_h\|_{1,\Omega_\mathrm{f}}$	$\|\phi-\phi_h\|_{0,\Omega_\mathrm{f}}$	$\|\underline{\chi}-\underline{\chi}_h\|_{0,\Omega_\mathrm{f}}$	$\|\underline{\chi}-\underline{\chi}_h\|_{1,\Omega_\mathrm{f}}$
0	5.5e-4	3.2e-2	6.0e-3	1.7e-5	3.8e-4
1	1.8e-4	1.9e-2	3.4e-3	6.7e-6	2.5e-4
2	4.5e-5	9.4e-3	1.6e-3	1.8e-6	1.3e-4
3	1.1e-5	4.7e-3	7.8e-4	4.5e-7	6.5e-5
4	2.8e-6	2.4e-3	3.9e-4	1.1e-7	3.2e-5

TABLE 1. Convergence results for two infinite parallel planes; the flow problem is solved using the mixed Crouzeix–Raviart/$\mathbb{P}_0$ finite element and the advection–diffusion problem is solved using the divergence-free velocity field in the space D_h.

4.1. **Analytical test cases.** Two test cases with analytical solution are considered, first that where the fluid flows between two infinite parallel planes and then that where the fluid flows in a circular cylinder.

4.1.1. *Infinite parallel planes.* Consider two planes located at $z_3 = \pm a$. Set $\underline{e}_\alpha = \underline{e}_1$ in (5). Then, the solution to the flow problem is

$$\underline{u} = \tfrac{1}{2}(a^2 - z_3^2)\underline{e}_1 \qquad \text{and} \qquad \phi = 0, \tag{65}$$

and the solution to the advection–diffusion problem is

$$\underline{\chi} = (-\tfrac{1}{24}z_3^4 + \tfrac{1}{12}a^2 z_3^2 - \tfrac{7}{360}a^4)\underline{e}_1. \tag{66}$$

All the coefficients of the diffusion and dispersion tensors vanish except

$$D_{11}^{\mathrm{diff}} = \varphi \qquad \text{and} \qquad D_{11}^{\mathrm{disp}} = \tfrac{2}{945}\varphi a^6, \tag{67}$$

where $\varphi = 2a$ is the porosity.

Two-dimensional simulations are performed on the plane $\{z_2 = 0\}$ and for $a = 0.3$. Table 1 presents convergence results for the discrete Stokes problem (42) and the discrete advection–diffusion equation (57) in which $\underline{w}_h = \underline{u}_h^{\mathrm{BDM}}$. The meshes are uniformly refined with maximum mesh-size $h_i = h_0 2^{-i}$ with $i \in \{0, \ldots, 4\}$ and $h_0 = 0.2$. We observe that the convergence orders match theoretical predictions. Similar convergence orders are observed if the flow problem is approximated using (40).

4.1.2. *Circular cylinder.* Consider a circular cylinder with radius a and generatrix parallel to $\underline{e}_1$. Set $\underline{e}_\alpha = \underline{e}_1$ in (5). Then, the solution to the flow problem is

$$\underline{u} = \tfrac{1}{4}(a^2 - r^2)\underline{e}_1 \qquad \text{and} \qquad \phi = 0, \tag{68}$$

with $r^2 = z_2^2 + z_3^2$, and the solution to the advection–diffusion problem is

$$\underline{\chi} = (-\tfrac{1}{64}r^4 + \tfrac{1}{32}a^2 r^2 - \tfrac{1}{96}a^4)\underline{e}_1. \tag{69}$$

All the coefficients of the diffusion and dispersion tensors vanish except

$$D_{11}^{\mathrm{diff}} = \varphi \qquad \text{and} \qquad D_{11}^{\mathrm{disp}} = \tfrac{1}{3072}\varphi a^6, \tag{70}$$

where $\varphi = \pi a^2$ is the porosity.

Three-dimensional simulations are performed for $a = 0.3$. Table 2 presents convergence results; the same finite element techniques as in Table 1 are used.

	Stokes			advection–diffusion	
i	$\|\underline{\boldsymbol{u}} - \underline{\boldsymbol{u}}_h\|_{0,\Omega_\mathrm{f}}$	$\|\underline{\boldsymbol{u}} - \underline{\boldsymbol{u}}_h\|_{1,\Omega_\mathrm{f}}$	$\|\phi - \phi_h\|_{0,\Omega_\mathrm{f}}$	$\|\underline{\chi} - \underline{\chi}_h\|_{0,\Omega_\mathrm{f}}$	$\|\underline{\chi} - \underline{\chi}_h\|_{1,\Omega_\mathrm{f}}$
0	1.1e-4	3.0e-3	6.7e-4	1.2e-6	3.5e-5
1	2.7e-5	1.6e-3	3.2e-4	3.5e-7	2.0e-5
2	7.1e-6	8.4e-4	1.4e-4	9.1e-8	1.0e-5
3	1.8e-6	4.6e-4	7.5e-5	3.1e-8	5.6e-6

TABLE 2. Convergence results for a circular cylinder; the flow problem is solved using the mixed Crouzeix–Raviart/$\mathbb{P}_0$ finite element and the advection–diffusion problem is solved using the divergence-free velocity field in the space D_h.

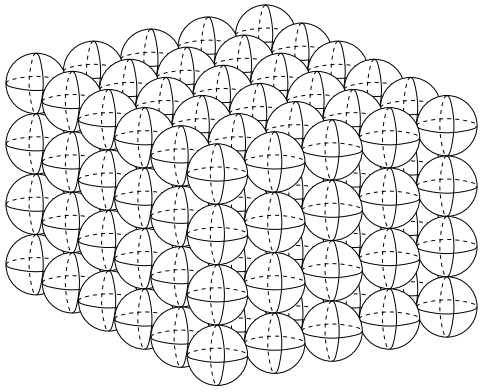

FIGURE 2. Three-dimensional cubic network of spheres.

The meshes are uniformly refined with maximum mesh-size $h_i = h_0 2^{-i}$ with $i \in \{0, \ldots, 3\}$ and $h_0 = 0.1$. We observe that the convergence orders are close to theoretical predictions.

4.2. **Cubic sphere networks.** The porous medium now consists of a cubic network of spheres such as the one illustrated in Figure 2. To avoid singular mesh elements, the spheres are not tangent, but their radius a is larger than 0.5. This also allows us to vary the porosity. The contact area between two adjacent spheres is a circle whose radius is denoted by ϱ. Figure 3 illustrates the mesh of the fluid domain Ω_f in the case $\varrho = 0.1$.

To investigate the impact of advection on the values taken by the diffusion and dispersion tensors, we solve (57) by scaling the discrete velocity field $\underline{\boldsymbol{w}}_h$ by the numerical factor λ. The values of the diffusion and dispersion tensors are then plotted as a function of $\lambda\Upsilon_\mathrm{av}$ where Υ_av denotes the norm of the average velocity within the pore. Recall that λ can take values between 0 and $\frac{1}{\Upsilon_\mathrm{max}}$; see (21). The constant Υ_max, which is the maximum norm of the velocity solving (5)–(8), depends on the shape of the fluid domain Ω_f and is generally of the order of 10^{-2}–10^{-3};

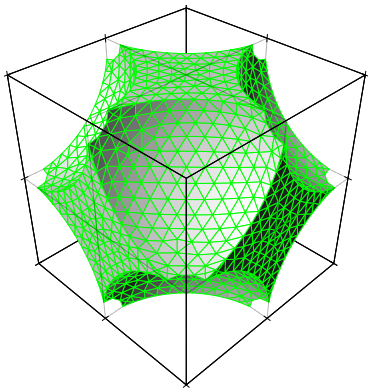

FIGURE 3. Mesh of the fluid domain Ω_{f} in the case $\varrho = 0.1$.

	$\Upsilon_{\max}$, $h = 0.05$		$\Upsilon_{\max}$, $h = 0.025$		Υ_{av}, $h = 0.025$	
ϱ	$\underline{u}_h^{\mathrm{Lag}}$	$\underline{u}_h^{\mathrm{CR}}$	$\underline{u}_h^{\mathrm{Lag}}$	$\underline{u}_h^{\mathrm{CR}}$	$\underline{u}_h^{\mathrm{Lag}}$	$\underline{u}_h^{\mathrm{CR}}$
0.1	2.36e-2	2.38e-2	2.37e-2	2.37e-2	4.86e-3	4.77e-3
0.3	1.08e-2	1.14e-2	1.13e-2	1.14e-2	1.63e-3	1.58e-3

TABLE 3. Maximum velocity norm $\Upsilon_{\max}$ and norm of average velocity Υ_{av} for the two pore morphologies evaluated by solving (40) or (42).

see Table 3 below. Hereafter, we vary λ in the range $[0, 10^3]$ independently of the morphology of the porous medium, keeping in mind that in some cases, the larger values may fall slightly beyond the strict validity domain of the theoretical framework.

Two cubic networks of spheres are considered, one with parameter $\varrho = 0.3$ (the sphere radius is $a = 0.583$ and the porosity is $\varphi = 0.244$) and one with parameter $\varrho = 0.1$ (the sphere radius is $a = 0.510$ and the porosity is $\varphi = 0.448$). For both geometries, two quasi-uniform simplicial meshes are constructed, a coarse mesh with mesh-size parameter $h = 0.05$ and a fine mesh with mesh-size parameter $h = 0.025$. For $\varrho = 0.1$, the coarse (resp., fine) mesh contains 14,626 (resp., 120,082) tetrahedra, while for $\varrho = 0.3$, the coarse (resp., fine) mesh contains 11,483 (resp., 60,112) tetrahedra. Observe that the meshes used for $\varrho = 0.3$ are somewhat coarser than those used for $\varrho = 0.1$.

Table 3 presents the maximum velocity norm $\Upsilon_{\max}$ and the norm of the average velocity Υ_{av} obtained with the two pore morphologies when solving (40) or (42). Results obtained on the coarse and fine meshes are reported for $\Upsilon_{\max}$, showing that $\underline{u}_h^{\mathrm{Lag}}$ is not yet very accurate on the coarse mesh for $\varrho = 0.3$. Furthermore, the values obtained for $\Upsilon_{\max}$ and Υ_{av} confirm that it is reasonable to use values of λ up to 10^3. We also observe that $\Upsilon_{\max}$ is five to ten times larger than Υ_{av}.

Table 4 presents the minimum linear system residual attained by GMRes for the two pore morphologies when solving (57) with $\underline{u}_h^{\mathrm{Lag}}$, $\underline{u}_h^{\mathrm{CR}}$, or $\underline{u}_h^{\mathrm{BDM}}$. The tolerance

	$h = 0.05$			$h = 0.025$		
ϱ	$\underline{u}_h^{\mathrm{Lag}}$	$\underline{u}_h^{\mathrm{CR}}$	$\underline{u}_h^{\mathrm{BDM}}$	$\underline{u}_h^{\mathrm{Lag}}$	$\underline{u}_h^{\mathrm{CR}}$	$\underline{u}_h^{\mathrm{BDM}}$
0.1	1.7e-3	4.0e-4	9.9e-7	1.7e-4	3.6e-5	5.3e-7
0.3	9.3e-4	3.7e-4	5.7e-7	1.8e-4	6.0e-5	3.0e-7

TABLE 4. Minimum linear system residual attained by GMRes for the two pore morphologies when solving (57) with $\underline{u}_h^{\mathrm{Lag}}$, $\underline{u}_h^{\mathrm{CR}}$, or $\underline{u}_h^{\mathrm{BDM}}$.

for solving the Stokes problem is set to 10^{-9}. When solving the advection–diffusion problem, the parameter λ is set to 10^3 to emphasize the effects of the non-zero divergence of the discrete velocity field. Results obtained on the coarse and fine meshes are reported. In both cases, the minimum value for $\underline{u}_h^{\mathrm{CR}}$ is an order of magnitude smaller than that for $\underline{u}_h^{\mathrm{Lag}}$. Moreover, the minimum value for $\underline{u}_h^{\mathrm{BDM}}$ is two orders of magnitude smaller than that for $\underline{u}_h^{\mathrm{CR}}$.

Tables 5 (resp., 6) presents the values taken by the diffusion (resp., dispersion) coefficients D_{11}^{diff} and D_{22}^{diff} (resp., D_{11}^{disp} and D_{22}^{disp}) for the two pore morphologies when solving (57) with $\underline{u}_h^{\mathrm{Lag}}$, $\underline{u}_h^{\mathrm{CR}}$, or $\underline{u}_h^{\mathrm{BDM}}$. Results obtained on the coarse and fine meshes are reported. The data for the Stokes problem is $\underline{e}_\alpha = (1, 0, 0)$, and the parameter λ is set to 10^3 to emphasize the effects of advection on the diffusion and dispersion tensors and to study the sensitivity of the predicted values for these tensors to the accuracy of the discrete velocity field. For the diffusion tensor, the three discrete velocity fields yield fairly accurate values (errors within a few percent) even on the coarse mesh for both geometries. For the dispersion tensor, the results lead to different conclusions. In all cases, the dispersion tensor evaluated with $\underline{u}_h^{\mathrm{Lag}}$ is inaccurate, even on the fine mesh. This is due to the fact that the total number of degrees of freedom needed to compute $\underline{u}_h^{\mathrm{Lag}}$ is $4N_{\mathrm{ve}}$, where N_{ve} is the number of mesh vertices, which is much less than that needed to compute $\underline{u}_h^{\mathrm{CR}}$ which is $N_{\mathrm{te}}+3N_{\mathrm{fa}}$ where N_{te} is the number of mesh tetrahedra and N_{fa} the number of mesh faces. Furthermore, the accuracy of the dispersion tensors computed using $\underline{u}_h^{\mathrm{CR}}$ and $\underline{u}_h^{\mathrm{BDM}}$ is similar, $\underline{u}_h^{\mathrm{CR}}$ yielding slightly more accurate results for D_{11}^{disp} (especially on coarse meshes) and $\underline{u}_h^{\mathrm{BDM}}$ yielding more accurate results for D_{22}^{disp} (especially for $\varrho = 0.3$). Thus, from a practical viewpoint, it seems sufficient to work with $\underline{u}_h^{\mathrm{CR}}$, though the advantage of using $\underline{u}_h^{\mathrm{BDM}}$ is that the discrete advection–diffusion problem is *granted* to be solved with high accuracy.

Figures 5 and 4 present for the two pore morphologies the values taken by the diffusion and dispersion tensors, respectively, as a function of $\lambda\Upsilon_{\mathrm{av}}$. Recall that in the advection dominated regime, the value of $\lambda\Upsilon_{\mathrm{av}}$ should be smaller than one and not too small. Simulations are performed with mesh-size $h = 0.05$, and (57) is solved using the divergence-free velocity field $\underline{u}_h^{\mathrm{BDM}}$. The dispersion coefficients D_{11}^{disp} and D_{22}^{disp} roughly scale as $(\lambda\Upsilon_{\mathrm{av}})^2$.

		D_{11}^{diff}			D_{22}^{diff}		
ϱ	h	$\underline{u}_h^{\text{Lag}}$	$\underline{u}_h^{\text{CR}}$	$\underline{u}_h^{\text{BDM}}$	$\underline{u}_h^{\text{Lag}}$	$\underline{u}_h^{\text{CR}}$	$\underline{u}_h^{\text{BDM}}$
0.1	0.05	3.56e-1	3.65e-1	3.67e-1	3.12e-1	3.13e-1	3.13e-1
0.1	0.025	3.57e-1	3.60e-1	3.60e-1	3.08e-1	3.09e-1	3.09e-1
0.3	0.05	1.37e-1	1.40e-1	1.40e-1	1.25e-1	1.25e-1	1.25e-1
0.3	0.025	1.36e-1	1.37e-1	1.37e-1	1.23e-1	1.23e-1	1.23e-1

TABLE 5. Diffusion coefficients D_{11}^{diff} and D_{22}^{diff} for the two pore morphologies evaluated by solving (57) with $\underline{u}_h^{\text{Lag}}$, $\underline{u}_h^{\text{CR}}$, or $\underline{u}_h^{\text{BDM}}$.

		D_{11}^{disp}			D_{22}^{disp}		
ϱ	h	$\underline{u}_h^{\text{Lag}}$	$\underline{u}_h^{\text{CR}}$	$\underline{u}_h^{\text{BDM}}$	$\underline{u}_h^{\text{Lag}}$	$\underline{u}_h^{\text{CR}}$	$\underline{u}_h^{\text{BDM}}$
0.1	0.05	1.85e-1	2.26e-1	2.36e-1	1.60e-3	2.77e-3	3.08e-3
0.1	0.025	2.12e-1	2.19e-1	2.21e-1	2.44e-3	2.85e-3	2.92e-3
0.3	0.05	2.13e-2	2.78e-2	3.05e-2	6.49e-5	9.72e-5	1.17e-4
0.3	0.025	2.44e-2	2.68e-2	2.77e-2	9.11e-5	1.12e-4	1.18e-4

TABLE 6. Dispersion coefficients D_{11}^{disp} and D_{22}^{disp} for the two pore morphologies evaluated by solving (57) with $\underline{u}_h^{\text{Lag}}$, $\underline{u}_h^{\text{CR}}$, or $\underline{u}_h^{\text{BDM}}$.

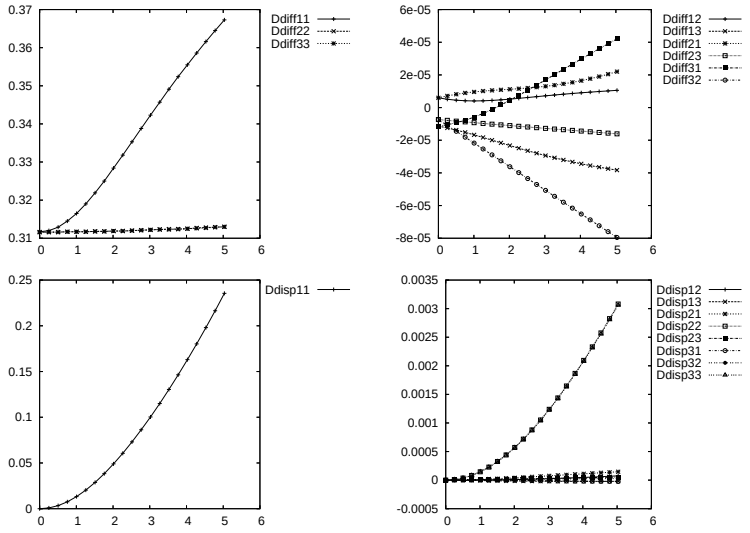

FIGURE 4. Cubic network of spheres with parameter $\varrho = 0.1$; diffusion (upper row) and dispersion (lower row) tensors as a function of $\lambda \Upsilon_{\text{av}}$.

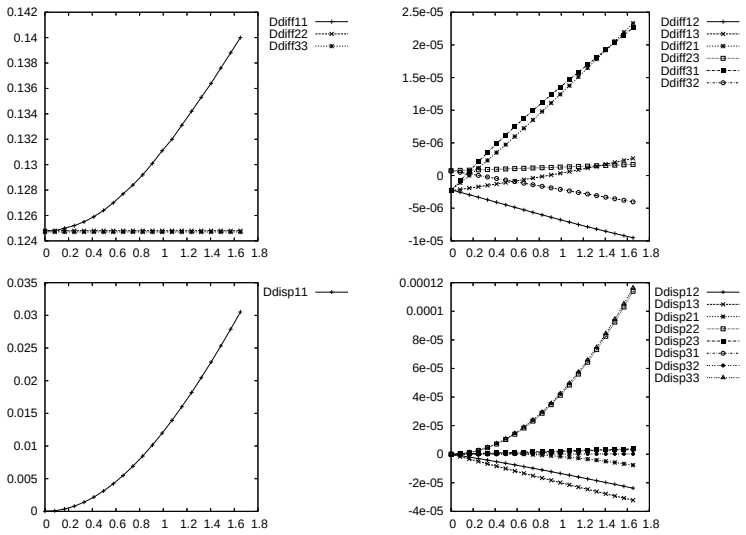

FIGURE 5. Cubic network of spheres with parameter $\varrho = 0.3$; diffusion (upper row) and dispersion (lower row) tensors as a function of $\lambda \Upsilon_{\mathrm{av}}$.

Finally, we consider a centered cubic network of spheres. The spheres located at the cube vertices have radius $a = 0.57$ while the sphere located at the center of the cube has radius $a = 0.15$. The resulting porosity is $\varphi = 0.262$. Results are obtained on a mesh containing 41,208 tetrahedra. The maximum velocity norm $\Upsilon_{\max}$ and the norm of the average velocity Υ_{av} are respectively equal to 1.0e-2 and 1.6e-3. The diameter of the spheres in the centered cubic network have been chosen so that Υ_{av} takes approximately the same value as for the cubic network with $\varrho = 0.3$; see Table 3. Figure 6 presents the values taken by the diffusion and dispersion tensors as a function of $\lambda \Upsilon_{\mathrm{av}}$. Comparing the pore morphology with an obstacle (the centered cubic network) to the pore morphology without an obstacle (Figure 5), we observe that D_{11}^{disp} is about 20% smaller while D_{22}^{disp} is up to six times larger, indicating that the presence of obstacles enhances transverse dispersive effects.

5. Conclusions

In the present work we have designed and analyzed a finite element tool to evaluate quantitatively diffusion and dispersion tensors in the presence of advection for various three-dimensional pore morphologies. The analysis shows that the most robust approach consists of approximating the velocity field using the mixed Crouzeix–Raviart/$\mathbb{P}_0$ finite element and then to construct a divergence-free discrete velocity field in the Brezzi–Douglas–Marini finite element space to solve the vector-valued advection–diffusion equation. From a practical viewpoint, the present numerical experiments indicate that the estimates for the diffusion and dispersion tensors are generally accurate enough without postprocessing the Crouzeix–Raviart

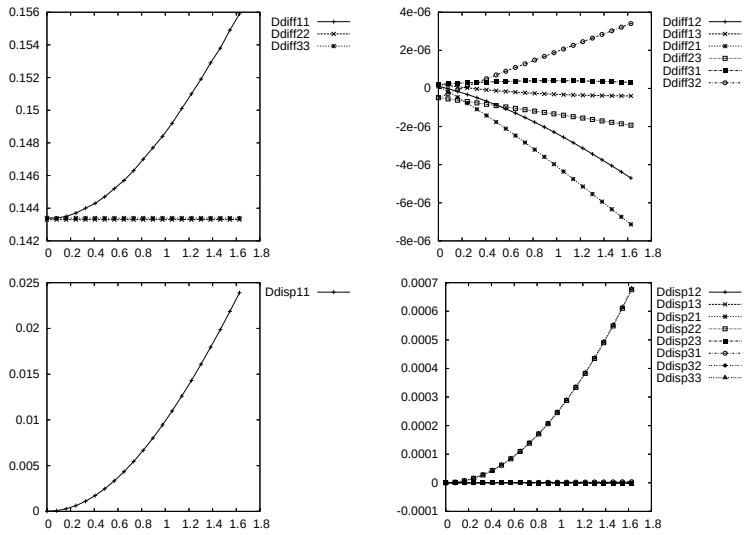

FIGURE 6. Centered cubic network of spheres with porosity $\varphi = 0.262$; diffusion (upper row) and dispersion (lower row) tensors as a function of $\lambda \Upsilon_{\mathrm{av}}$.

velocity field. On the contrary, working with stabilized finite elements to approximate the velocity field often yields insufficient accuracy, especially when evaluating the transversal components of the dispersion tensor.

Acknowledgment. Access to the three-dimensional mesh generator Tetmesh–GHS3D at the University of Metz was granted in the framework of the GdR MOMAS (CNRS–2439, ANDRA, BRGM, CEA, EdF).

REFERENCES

[1] P.W. Atkins. *Physical chemistry*. Oxford University Press, 1992.

[2] J.-L. Auriault. Transport in porous media; upscaling by multiscale asymptotic expansions. In L. Dormieux and F.-J. Ulm, editors, *Applied micromechanics of porous materials, CISM Courses and Lectures n. 480*. Springer, Wien, NewYork, 2005.

[3] J.-L. Auriault and Y. Lewandowska. Diffusion/adsorption/advection macrotransport in soils. *Eur. J. Mech. A/Solids*, 15:681–704, 1996.

[4] P. Bastian and B. Rivière. Superconvergence and $H(\mathrm{div})$ projection for discontinuous Galerkin methods. *Internat. J. Numer. Methods Fluids*, 42(10):1043–1057, 2003.

[5] J. Bear and Y. Bachmat. *Introduction to the Modelling of Transport Phenomena in Porous Media*. Kluwer Academic Publishers, 1990.

[6] F. Brezzi, J. Douglas, Jr., and L.D. Marini. Two families of mixed finite elements for second order elliptic problems. *Numer. Math.*, 47(2):217–235, 1985.

[7] L. Dormieux and D. Kondo. Diffusive transport in disordered media. Application to the determination of the tortuosity and the permeability of cracked material. In L. Dormieux and F.-J. Ulm, editors, *Applied micromechanics of porous materials, CISM Courses and Lectures n. 480*. Springer, Wien, NewYork, 2005.

[8] H. Ene and E. Sanchez-Palencia. Equations et phénomènes de surface pour l'écoulement dans un modèle de milieu poreux. *Journal de Mécanique*, pages 73–108, 1975.

[9] A. Ern and J.-L. Guermond. *Theory and Practice of Finite Elements*, volume 159 of *Applied Mathematical Sciences*. Springer-Verlag, New York, NY, 2004.

[1]CERMICS, Ecole nationale des ponts et chaussées, Champs sur Marne, 77455 Marne la Vallée Cedex 2, France

[2]LMSGC, Ecole nationale des ponts et chaussées, Champs sur Marne, 77455 Marne la Vallée Cedex 2, France
E-mail address: pierredh@cermics.enpc.fr
E-mail address: ern@cermics.enpc.fr
E-mail address: dormieux@lmsgc.enpc.fr